

Date of publication xxxx 00, 0000, date of current version xxxx 00, 0000.

Digital Object Identifier 10.1109/ACCESS.2017.DOI

Direct Signal Encoding with Analog Resonate-and-Fire Neurons

HENDRIK M. LEHMANN^{1,3}, JULIAN HILLE^{2,3}, CYPRIAN GRASSMANN³ AND VADIM ISSAKOV^{1,3}

¹Institute of CMOS Design, Technical University of Braunschweig, Germany

²Department of Informatics, Technical University of Munich, Germany

³Infineon Technologies AG, Neubiberg, Germany

Corresponding author: Hendrik M. Lehmann (e-mail: hendrik.lehmann@infineon.com).

This work was funded by the German Federal Ministry of Education and Research (BMBF) within the KI-ASIC project (16ES0992K). We thank Infineon Technologies AG for supporting this research.

ABSTRACT Sensors are an essential element in a wide range of applications. As the number of sensors increases, so does the amount of data collected with them. This raises the challenge of efficiently processing this data. Spiking Neural Networks (SNNs) represents a promising approach to solve this problem through event-based, parallelized data processing. For SNNs to be genuinely efficient, some fundamental challenges arise, like converting analog signals to spike events. An emerging possibility is the use of Resonate-and-Fire (R&F) neurons, capable of reacting to specific frequency components of input signals. In this work, we present a possible analog implementation for a R&F neuron and show the practical encoding of analog signals into a spiking domain using actual measurements. The coding method allows analog sensor signals to be directly applied to SNNs for efficient data processing. In the future, this approach can potentially enable the direct integration of analog Spiking Neural Networks into sensors.

INDEX TERMS Sensor, Spiking Neural Networks, Neuromorphic Hardware, Signal Encoding

I. INTRODUCTION

SENSORS are an important component of automation and data collection. With a higher degree of automated driving, various sensor modalities consume power, limiting the travel range. The computation performance and power consumption constrain the real-time processing of the sensor data. Thus, this simple question arises: *How can we process this data more efficiently?*

One promising approach is the application of data-driven Neural Networks (NNs) [1]. The 3rd generation networks model the biological counterpart and promise a significant energy reduction through event-and parallel processing [2]. In contrast to traditional NN, SNNs use spike events to transmit information across the network instead of floating point values, providing two advantages: 1) the event-based processing, 2) the reduced binary communication [3].

Since the spiking networks use binary events, we must encode our signals to spatio-temporal spikes [4]. Different encoding methods can be realized on the digitized signal or directly on the analog signal. With traditional networks on digital hardware, there was no motivation to remove the analog-to-digital conversion. However, the spiking networks

on analog hardware promise a high energy efficiency [5].

The digital world argues the fact that a wide range of solutions of neural accelerators already exists [6]–[11]. In addition, the general process of converting the analog signal to the digital signal is a standard procedure in many application areas today and can thus be easily made suitable for this purpose. Contrary to this is the fact that a digital conversion always requires additional energy; it can lead to quantization errors and translation errors. A compromise between the sampling rate and frequency of the input signal must always be made [12]. In favor of the analog approach is the fact that the complete analog to the digital path can be bypassed, and in principle, the energy consumption can be reduced. In addition, the analog domain enables real asynchronous and event-processing while utilizing the local memories [13]. A review of digital and analog neuromorphic hardware is presented by [14], where the analog implementations demonstrate a faster processing. The drawback is insufficient research attention to methods for analog-to-spike conversion.

Nevertheless, the idea of direct signal processing is very promising. Therefore, we present, to the best of the author's knowledge, for the first time an analog implementation of

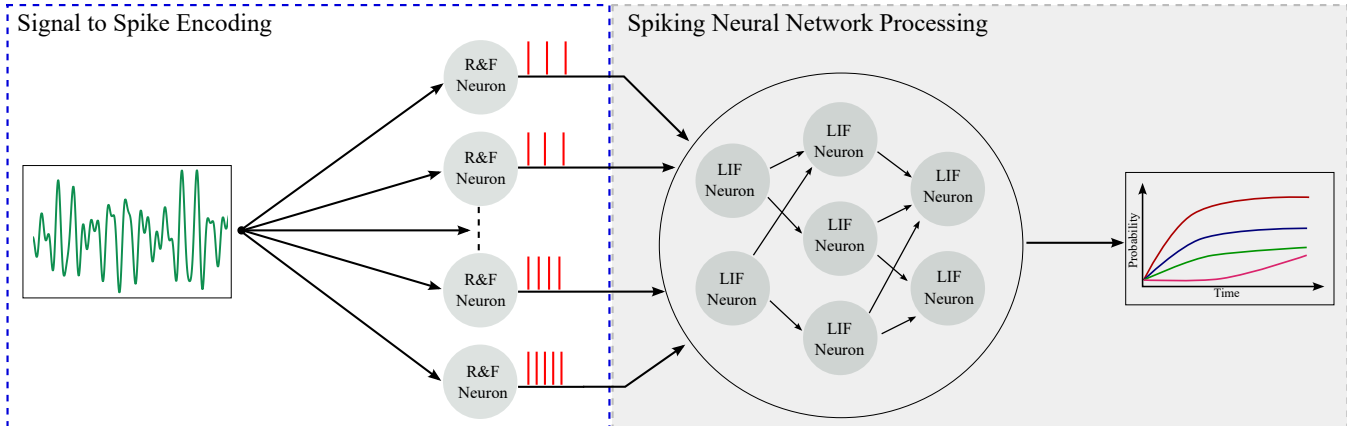


FIGURE 1: Conceptual representation of a potential signal processing chain for Spiking Neural Network (SNN). The input signal is translated into spikes by the Resonate-and-Fire (R&F) neurons. The encoded signal is then passed to the subsequent SNN for processing. At last, the evaluation is done by a feasible decoding method. In this work, we consider the signal to spike translation.

the R&F neuron for the direct frequency-dependent analog to spike conversion. We base our assumptions on the neuron model of the R&F neuron introduced by Izhikevich in 2001 [15]. Unlike other neuron models, it offers the features of natural frequency selectivity. Simply, a resonant frequency results in a translation to spikes at the same frequency. By combining differently tuned R&F neurons, a signal can thus be split to the different frequency components [16], [17]. Figure 1 shows a schematic of the R&F encoding with the directly connected input signal and an example subsequent network. The proposed implementation of an analog circuit is based on common standard circuits such as a bandpass filter and a comparator. We implemented the circuit in a 130nm CMOS process. We have added the possibility of adjusting the resonance frequency and the Q-factor of the bandpass filter. This adaptability allows using a single circuit for different resonant frequencies, providing the flexibility of dynamic resonance frequency adjustment depending on the application. Additionally, to the simulations, we confirm the functionality by measuring the direct encoding of analog signals into spike events.

The paper is organized as follows. First, we describe the current state of the art in I-A and address the theoretical and mathematical principles for the R&F neuron and encoding method used in II. Afterwards, we describe in III the circuit design for the R&F neuron and demonstrate the functionality of the circuit with simulative examples. Next, in IV, we use a fabricated test chip to verify our simulative considerations by measurements. Finally, we discuss in V advantages of our work as well as their limitations.

A. STATE OF THE ART

This section first analyzes popular encoding methods for SNNs. Then, we consider previous implementations of R&F neurons as analog and digital implementations. For a comprehensive overview of encoding schemes, we refer to [18].

There is no single encoding scheme for all data types, which was also shown by biological experiments [19]–[22]. The current methods can be categorized into the rate and temporal codes [18], [23]. Rate codes use the spike frequency as the primary information source, while temporal codes use mainly the temporal correlation to a global or local reference. Traditional NNs like CNNs, LSTMs, and more are an approximation of the rate-based encoding scheme, meaning that these architectures can be converted to SNNs [24]. One big drawback of rate codes is the power consumption since analog or event-driven hardware only consumes power during a spike.

Temporal codes like the time-to-first spike (TTFS) utilize the time between the global reference and the spikes are more promising because of the lower spike count. An early spike indicates a high level, while a later spike is less important. Replacing the reference with an oscillation and defining the sinusoidal peak as the reference is called phase code [25]. Another temporal encoding is temporal contrast (TC) which converts a continuous signal into a spike train through signal intensity changes. Thus, positive and negative spikes represent the polarity of change. Such an encoding occurs in an event-based vision sensor with a high dynamic range [26].

We study in this paper a filter-based TC approach called current injection. In the literature several examples can be found which use such approach to convert analog signals into spike domain [27]–[30]. The common aspect of these methods of conversion is that the main information of the signal is represented by the amplitude. A frequency information can be partially conserved if exact knowledge about the corresponding input signal is known and the subsequent neuron is appropriately parameterized to this signal, as shown in [27]. This loss of information can be compensated by using R&F neurons. In [16], the authors show that R&F neurons can be used to study temporal signals in the frequency domain. The authors use the example of an FFT for this purpose.

The signals are fed through a layer based on R&F neurons. The neurons act as filter banks and select corresponding frequency components depending on the parameters of each neuron. The neuron converts the frequency component into a spike train with the corresponding frequency.

Important to note is the differentiation of the encoding schemes for frame-based or continuous data. The research community defines frame-based as periodical data like images, and continuous data are analog signals from pixels, audio signals, or temperature sensors. The requirements for real-time depend highly on the data. Rate or TTFS coding is less suitable for continuous data since a representation of the continuous data requires a representation that defines each value into a subsequence. Thus, not every encoding applies to all kinds of data.

Two analog implementations can be found in the literature for a R&F neuron. The first implementation is based on a derivation by a Volterra system [31]. This implementation shows some properties for a R&F neuron. However, the circuit does not show the desired parameterization of a R&F neuron, which is necessary for flexible encoding. Additionally, no post-silicon circuit verification is performed, so it provides limited information about the actual functionality. In the second realization, an implementation of the R&F neuron is shown, based on so-called fixed magnetic skyrmions [32]. This implementation provides an energy-efficient implementation for a R&F neuron. However, the frequency range for this implementation is limited to a low GHz range. Additionally, no standard CMOS circuitry is implemented by this approach, which strongly limits the access for replications. Furthermore, there is also no post-silicon verification. Finally, a digital implementation with the neuromorphic research processor Loihi 2 can be found in the literature [33]. Since we want to directly encode analog signals into spikes, this has no further relevance. However, we note that any software-based neuromorphic processor can implement digital R&F neurons.

II. THEORETICAL BACKGROUND

In this section, we first describe the mathematical theory behind the R&F neuron. Then, we address an ideal encoding scheme with R&F neurons.

A. MATHEMATICAL DESCRIPTION OF THE RESONATE-AND-FIRE NEURON

The R&F neuron of Izhikevich [15] is a neuron model where a damped oscillation models the membrane potential. If the resonant oscillation exceeds the neuron threshold, it emits a spike due to an amplification of the frequency, meaning the neuron selects the frequency components that match the resonance. Accordingly, the membrane potential oscillates stronger for input frequencies close to the neuron resonance frequency. The complex neuron is a two-dimensional linear

system defined by Izhikevich as:

$$\dot{x} = bx - \omega y, \quad (1)$$

$$\dot{y} = \omega x - by, \quad (2)$$

where x is the current-like variable and corresponds to the real component of the complex oscillation. The y variable describes the imaginary component, the voltage-like variable. The angular velocity $\omega = 2\pi \cdot f_0$ defines the resonant frequency of the neuron. Due to the damping factor b , the neuron can forget the existence of an input frequency by decaying back to the resting potential. Also, the damping affects the increase of the neuron's oscillation amplitude. An equivalent complex representation can be derived from this:

$$\dot{z} = (b + i\omega)z, \quad (3)$$

Where $z = x + iy \in \mathbb{C}$ describe the complex-valued variables of the oscillatory behavior of the neuron. A corresponding output spike δ is generated whenever the voltage-like variable y exceeds a threshold θ :

$$\delta = \begin{cases} 1, & \text{if } y > \theta \\ 0, & \text{else.} \end{cases} \quad (4)$$

B. ENCODING WITH RESONATE-AND-FIRE NEURONS

As mentioned in I-A we follow the approach of the current-injection encoding. We explain shortly the principle on an example. In case of the R&F encoding, we combine a simultaneous time-to-frequency conversion and spike encoding. Therefore, a population of R&F neurons convert a low dimensional input signal into a spatial-temporal spike representation, where each neuron response to a different frequency.

Exemplary, we define a superposition of N sinusoidal input signals by:

$$S_{in} = \sum_{i=1}^N A_i \sin(2\pi \cdot f_i), \quad (5)$$

where A represents the amplitude and f the frequency of a sinusoidal signal. A single R&F neuron filters the signal which is closed to its resonant frequency. While a population of R&F neurons react on different frequency components.

If there is no neuron with a respective resonance frequency, the according frequency part will not be considered and therefore not encoded. However, this assumes that we consider an ideal system to describe the principle. This means that the bandwidth of a resonant frequency is not taken into account. We assume that only a signal component with the correct frequency part leads to the excitation of a corresponding neuron. This results in each neuron spiking at the resonant frequency, assuming it is excited as previously described. Accordingly, a translation from the temporal domain to a spiking domain of each sinusoidal component of the input signal S_{in} is performed. Each sinusoidal part is represented by a corresponding spike train as long as a corresponding frequency part is present.

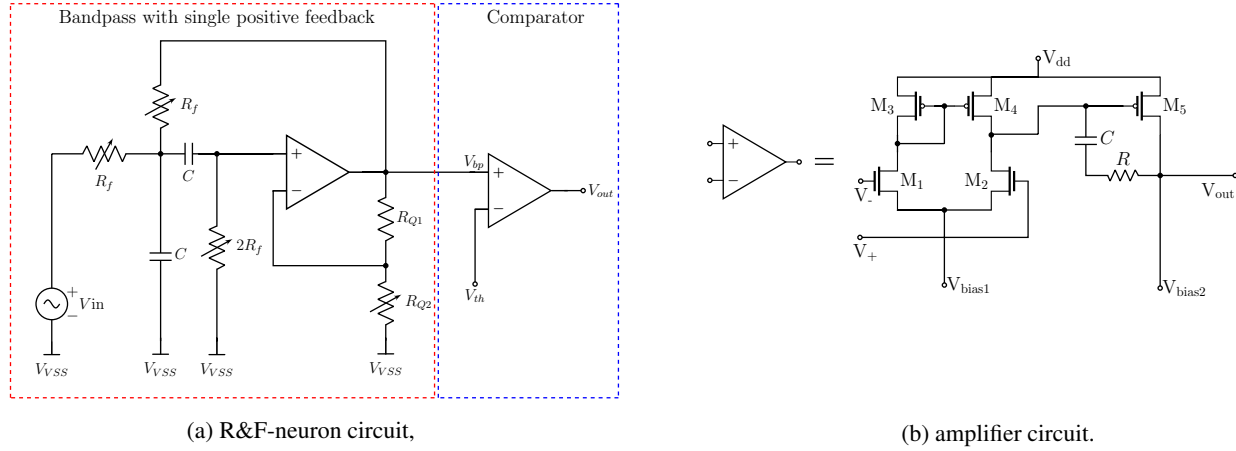


FIGURE 2: R&F circuit implementation. In a), we demonstrate the circuit for the R&F neuron. The circuit comprises a bandpass filter (blue) and a comparator (red). In b) the focus on the amplifier on a transistor level, used as bandpass and comparator.

III. CIRCUIT DESIGN CONSIDERATIONS

In the following, we first discuss the demands for a circuit implementation of a R&F neuron. We then describe the key circuit blocks and the complete circuit of the R&F neuron. We show complementary simulations of the described circuit blocks to study their functionality.

A. DEMANDS ON A CIRCUIT IMPLEMENTATION

We identify two basic requirements for a circuit design. First, we need selective frequency detection, and afterwards, we have to translate the frequency into a corresponding spike train with the same frequency.

Different possibilities exist for detecting a corresponding resonant frequency f_{res} . A logical approach is the realization of a resonance circuit, which swings when the input signal contains the circuit's resonance frequency. From this step, this can then be translated into a spike train. However, this intuitive step of a resonant circuit lures into a trap. For an integrated circuit, the requirement is to be area efficient. However, a resonant circuit is accompanied by either a large capacitance or a large inductance if the frequencies are set in a low MHz range. There are several possibilities to counteract this; for example, replacing the inductive part with a capacitive part with a gyrator circuit is possible [34]. This results in finding a trade-off between capacitor size and desired frequency.

Nevertheless, there is also another alternative. As mentioned at the beginning, an encoding network based on R&F neurons represents a selective filter bank for different frequency components. From this, the idea can be derived not to implement the resonance part as an actual resonator but to replace this with a narrowband bandpass filter. This solves the frequency selective filtering task according to the designed resonance frequency. For the implementation of bandpass filters, there are many ideas and approaches in the literature [35]–[38]. We use a bandpass with single positive feedback [36]. This has the advantage of a well-known circuit and does

not require inductive circuit components.

Similarly, we have found different approaches for translating a resonant frequency into a corresponding spike train [39]–[42]. We have chosen to implement a comparator circuit to enable a flexible threshold selection. When the oscillation exceeds the threshold, the output level is raised too high, generating a spike. If the amplitude falls below the threshold again, the level is lowered to the low level. This allows a simple translation into a spike train with the same period when the signal periodically exceeds the threshold, carrying the additional information of the signal's amplitude.

In order to implement a circuit concept for the R&F neuron, we combine this two fundamental circuit blocks. First, the frequency-selective behavior (resonate) uses the concept of a bandpass. With this circuit, desired frequencies are filtered out and amplified while unwanted frequencies are suppressed. Secondly, a comparator generates the spike (fire) output by comparison of the maximum decoupling of the resonating signal with a threshold value. Figure 2a shows the circuit of the neuron.

We have decided to use an efficient realization approach for a R&F neuron. Bandpass and comparator are, therefore, basic circuits that are well-known from the literature [36].

B. BANDPASS FILTER

The bandpass filter with single positive feedback, which we use here, is based on the circuit presented in [36]. In this case, the internal gain is set to the value of k by the negative feedback through the voltage divider $R_{Q1}(k - 1)$ and R_{Q2} . The derived transfer function can be used to find the dimensioning parameters for the circuit. The transfer function is, therefore:

$$A(P) = \frac{kR_fC\omega_r P}{1 + R_fC\omega_r(3 - k)P + R_f^2C^2\omega_r^2P^2}. \quad (6)$$

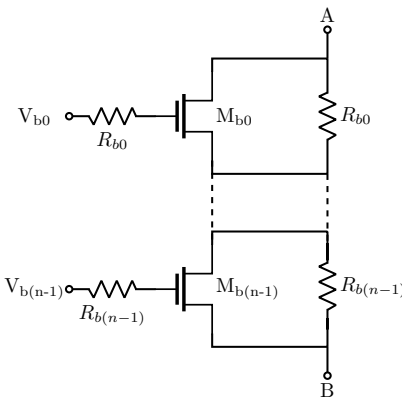


FIGURE 3: Circuit for adjustable resistor network. Both are used in the bandpass filter for the frequency selectivity and the adjustment of the Q-factor.

The resonant frequency of the circuit is directly proportional to R_f and C , thus the resonant frequency is defined as:

$$f_r = \frac{1}{2\pi R_f C}. \quad (7)$$

The quality factor Q and the gain A_r are not independent. In other words, the Q directly affects the gain. Nevertheless, the resonant frequency is not changed by a modification of k . In the following equations, the corresponding dimensionalization possibilities for the Q and gain can be obtained:

$$A_r = \frac{k}{3-k} \quad (8)$$

$$Q = \frac{1}{3-k} \quad (9)$$

Note, in designing the circuit, that a $k \geq 3$ results in an infinite gain or undamped oscillation. We designed the circuit to achieve a value of $k = 2.96$.

For the implementation of the active filter, we use a simple two-stage amplifier; see Figure 2b. The amplifier is designed to produce a maximum gain that is as homogeneous as possible over the desired, switchable resonant frequencies. In addition, we have added a capacitor in parallel with a resistor at the output of the amplifier. This allows us to have a sufficient phase reserve. The bias currents V_{bias1} and V_{bias2} are generated and fed via current mirrors. The complete circuit is driven by a supply voltage of $V_{dd} = 1.5$ V. In addition, a virtual ground potential must be introduced to ensure the circuit's functionality. We have designed the circuit for $V_{VSS} = \frac{V_{dd}}{2}$ and the ground signal V_{SS} .

The resistors for the resonant frequency have the same value of R_f . Only the resistor connected ahead of the amplifier has a value of $2R_f$. For a universal use of the neuron circuit, we consider the option of adjustability of the resonant frequency and the quality factor. The resistors for the resonance frequency (2-bit), as well as the quality factor (3-bit),

can be controlled digitally; see Figure 3. For this, the resistors are connected in series to each other and switched on or off via transistors. The tunability of the circuit via this method allows a compact layout. The used capacitors are integrated area-wise over the resistor network and the transistors.

C. COMPARATOR

After the frequency selectivity, we transform the signal from the time domain to the spike domain. We have implemented a comparator circuit based on the same amplifier circuit from the bandpass, visualized in Figure 2b. The amplified signal from the bandpass filter is connected with the non-inverting input of the amplifier. The threshold is applied to the inverting input. Unlike the bandpass filter, the reference potential is now V_{SS} again instead of V_{VSS} . This allows us to provide smoother integration with the subsequent circuit systems. However, the reference potential can be easily changed if necessary. We describe the operation of the comparator by the definition of the comparator's output signal V_{out} :

$$V_{out} = \begin{cases} 1.5 \text{ V, if } V_{bp} > V_{th} \\ 0 \text{ V, else,} \end{cases} \quad (10)$$

where V_{bp} represents the output signal of the bandpass and V_{th} defines the threshold. If the bandpass is inactive or the signal amplitude is below the threshold, the output signal is at “low” level, meaning $V_{out} = 0$ V. When the amplitude is large enough to exceed the threshold, the signal rises to the “high” level. Thus, the output voltage is set to V_{dd} such that $V_{out} = 1.5$ V is valid. The high level continues until the value falls below the threshold again. This means the pulse width directly depends on the selected threshold value and the oscillation amplitude. The closer the threshold value is to the maximum peak of the wave, the smaller the pulse width. In reverse, this results in the fact that if the threshold value is chosen to be the same for all R&F neurons, the pulse width is slightly different depending on the frequency chosen since the threshold is crossed at different times and held for different durations. [33] named the amplitude-dependent event graded spike.

D. RESONATE-AND-FIRE NEURON

Combined with the bandpass filter and the comparator, we arrive at the R&F neuron. Figure 2a depicts the complete circuit. Overall, the implementation has three adjustable parameters. 1) Two bits for the resonance frequency, resulting in four different resonances. 2) Three bits for the Q-factor, resulting in eight different Q-factor settings, and 3) a flexible threshold. The resonance frequencies cover the frequencies of 0.9–1.05 MHz, the Q-factor a range of $\Delta Q = 11$ dB and the threshold can be set from 0–1.5 V.

E. CIRCUIT SIMULATIONS

We performed AC simulations to investigate the bandpass behavior of the circuit. For this, we vary from 10 Hz–1 GHz. Figure 4a shows the filter in terms of the different resonant

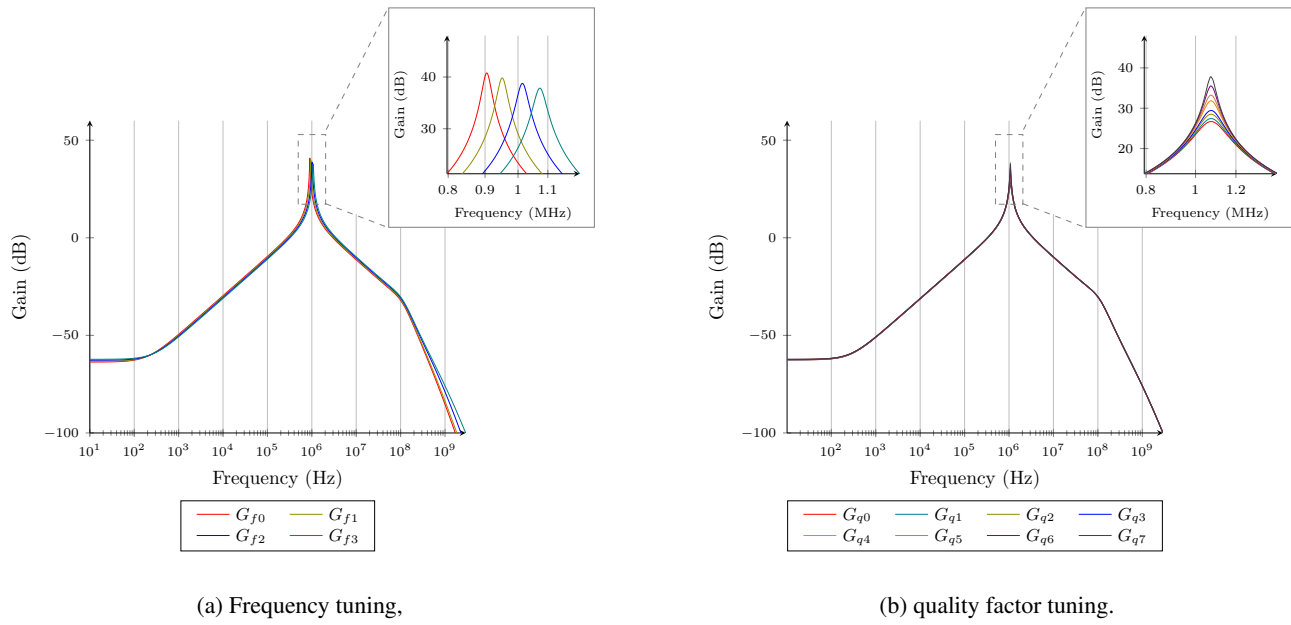


FIGURE 4: Simulation of the tuning options of the bandpass filter. In a), the adjustability of the frequencies over four different resonance points is shown. In contrast, in b), the adjustability of the quality factor in eight different levels is shown in the example of one resonance point.

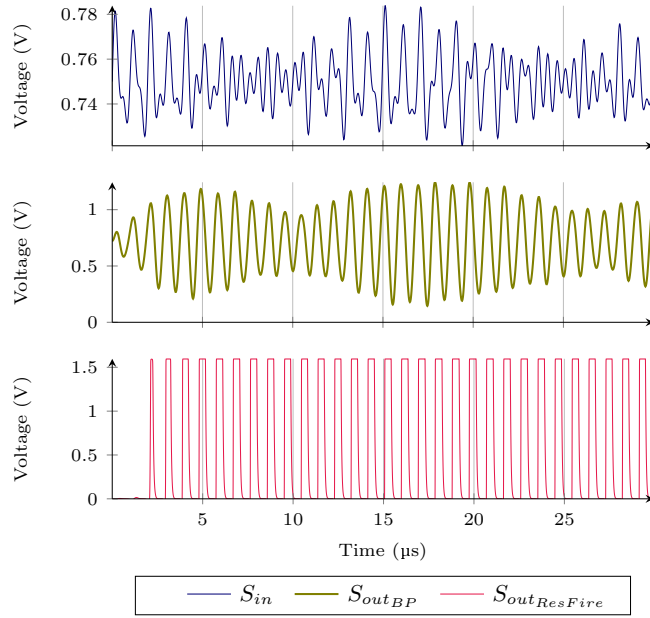
frequencies. We decided to design the frequency of the filter in such a way that the four possible resonant frequencies are at $G_{f0} = 905\text{ kHz}$, $G_{f1} = 960\text{ kHz}$, $G_{f2} = 1.015\text{ MHz}$ and $G_{f3} = 1.07\text{ MHz}$. The figure shows the maximum gain set for the respective resonance frequency. Thereby the maximum gain has a distance of about 55 kHz to each other. It can be seen that the higher the frequency, the lower the gain. However, the design of the circuit ensures that the gain is as homogeneous as possible. The gain of a filter proportionally influences the settling time.

In addition, we decided to provide the possibility to adjust the quality factor of the circuit. This results in three significant advantages. On the one hand, the quality with a value of $k = 2.96$ is chosen relatively close to the critical value for the possible overshoot of the system. Due to possible tolerance deviations and unwanted parasitic effects in manufacturing, the circuit may exceed the critical k value. The Q-factor can be reduced to counteract overshoot behavior in the fabricated chip. A lower Q-factor provides more system stability in general. On the other hand, a further advantage is that wider bandwidths are to be examined and/or used in later systems. The encoding is frequency selective, but exactly one frequency can never be chosen exclusively in a real system. Some bandwidth is always selected concerning the threshold, which is considered sufficient. A flexible bandwidth allows a more reasonably broad sampling of input frequencies. Finally, the Q-factor and the selected bandwidth influence the settling time of the circuit. The lower the quality, the faster the circuit settles to a particular frequency. For certain application areas, this could be an essential factor

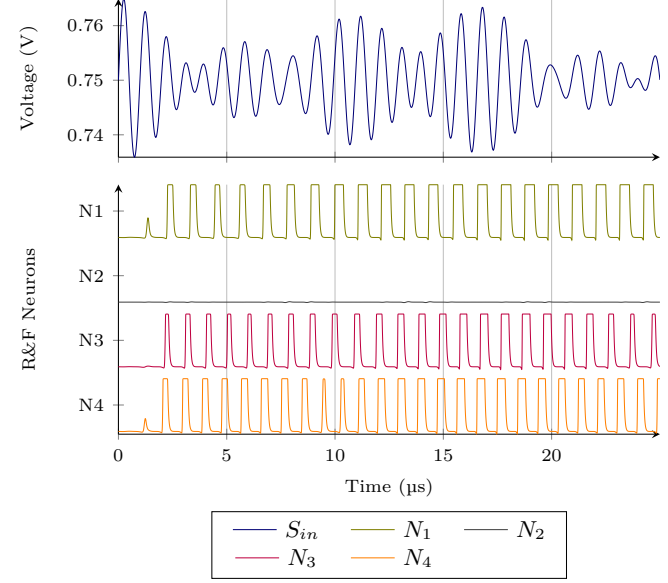
to minimize this time in order to be able to react quickly to certain frequency inputs. In this case, we have implemented eight possible settings for the Q-factor. This allows us to achieve a deviation from the maximum gain to the minimum gain of $\Delta G = 11\text{ dB}$ in this case. Figure 4b shows the tuning option for the Q-factor. Note that frequency selectivity or differentiation of input frequencies at lower bandwidths reduces resolution since resonant frequencies may be less distinguishable. Thus, the intersection of filtered frequencies increases thereby.

In the following, we investigate the R&F neuron by applying transient simulations. First, we focus on a single neuron. Subsequently, we demonstrate the previously described principle of current-injection encoding using R&F neurons on a set of four neurons.

In order to analyze a single neuron, the circuit is parameterized by choosing the highest Q-factor and the resonant frequency G_{f3} from Figure 4a. We examine a time window of $t = 30\mu\text{s}$ in Figure 5a. The input signal S_{in} is a superposed signal of two sinusoidal waves with a frequency of $f_1 = 1.01\text{ MHz}$ and $f_2 = 1.07\text{ MHz}$ with an amplitude of $V_{S_{in}} = 5\text{ mV}$ and an offset to V_{VSS} . We can observe the filtering of the frequency f_2 by the R&F neuron. Initially, the circuit needs a short settling time. After that, no ideal sine wave can be seen. We observe a signal with an uneven signal curve due to the uneven signal response caused by the signal mixing and define this as a signal leakage. However, this is not a problem for the neuron as long as the threshold value is chosen sufficiently. If the threshold is too high, there may be cases where individual periods are not converted into spikes.



(a) Single R&F neuron,



(b) Population of R&F neurons.

FIGURE 5: Transient simulation of a single R&F neuron as well as a population of four R&F neurons. In (a), we show the transient simulation of the single R&F neuron. The input signal is a superposition of two sinusoidal waves with a frequency of $f_1 = 1.01$ kHz and $f_2 = 1.07$ kHz. The neuron extracts the frequency f_1 and transforms it into spikes. In (b), we examine a population of four R&F neurons through an input signal, consisting of four sinusoidal waves with the frequencies $f_1 = 905$ kHz, $f_2 = 1.05$ MHz, $f_3 = 1.07$ MHz and $f_4 = 1.125$ MHz. As expected, the frequency $f_{1,2,3}$ are converted to spikes, f_4 is not considered due to the wrong resonant frequency of N_2 .

If the threshold is too low, unwanted frequency components may be translated into spikes. The correct trade-off for the threshold must be found, either through previously known signal characteristics or good training of the SNN for the threshold. In this case, the threshold is chosen so that each period results in an output spike.

In the second case, we consider a simulated input layer for a SNN based on four R&F neurons as depicted in Figure 5b. Each neuron is parameterized to use the highest Q-factor within the bandpass filter, and each neuron uses one resonant frequency from Figure 4a. In this case, an input signal S_{in} consisting of a superposition of four sinusoidal waves with the same amplitude and offset as previously injected into the system. We selected an observation time window of $t = 25$ μ s. The sinusoidal signals have a frequency of $f_1 = 850$ kHz, $f_2 = 910$ kHz, $f_3 = 1.01$ MHz, and $f_4 = 1.07$ MHz. In each case, we consider only the output signals of the individual neurons. It can be seen that the neurons N_1 , N_3 , and N_4 generate proper spike trains. In contrast, neuron N_2 remains at a low level throughout. This is because the input signal does not have the necessary frequency component to trigger this neuron ($G_{f1} = 960$ kHz). Instead, all other neurons are triggered. Another effect of signal leakage due to summing signals up can also be noticed. The neuron is triggered if the threshold is chosen so that the output signal exceeds the threshold. However, if the amplitude varies sufficiently to exceed the threshold, the result is that a spike

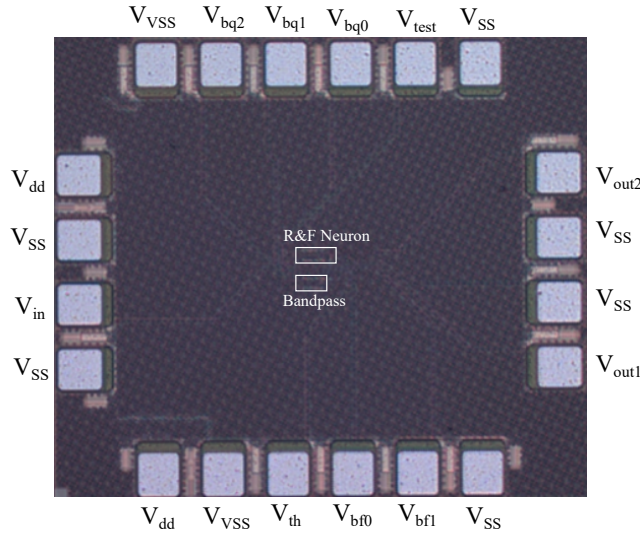
also varies in pulse width. An invariant spike is only given if the signal exceeds the threshold with the same amplitude width. However, this pulse width variation could be seen as a kind of graded spikes like used in [33].

IV. MEASUREMENTS

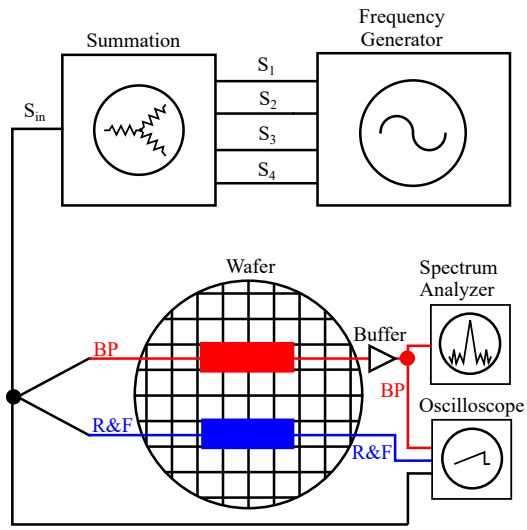
After the theory and simulative experiments, we verify the functionality with post-silicon measurements. Thus, we present the fabricated chip in a 130 nm BiCMOS process. Afterwards, we verify our observations from the simulations by post-silicon measurements.

A. FABRICATED CHIP

We validate our considerations for implementing a R&F neuron by post-silicon measurements. For this purpose, we have implemented the circuits for the R&F neuron as well as the bandpass stand-alone in a 130 nm BiCMOS process. However, as previously described, this is a straight CMOS design and thus can be transferred and scaled to any other process. The test chip has a total area consumption of $0.9 \text{ mm} \times 1 \text{ mm}$. The area consumption of the active region for the bandpass alone is $34 \mu\text{m} \times 85 \mu\text{m}$ and the entire R&F neuron consumes an area of $34 \mu\text{m} \times 100 \mu\text{m}$. The two circuits share the input signal pad and have an individual output pad for each circuit output. In addition to the supply voltages, the respective bits can be set manually for parameterization, and each bit-pad is shared between both circuits. The signal V_{test} is an internal



(a) Chip photography,



(b) Measurement setup.

FIGURE 6: A chip photography of the fabricated chip in a 130 nm process is shown in (a) and in (b) a block diagram of the used measurement setup for evaluation of the bandpass filter as well as the encoding principle with R&F neurons.

signal for checking correct functionality purposes and has no further significance for verification. Figure 6a shows a photograph of the manufactured chip.

Figure 6b presents a block diagram showing the measurement setup used for evaluating the test chip. We measure the circuit directly on wafer level. A frequency generator is used to generate either a single signal or four signals which are combined additively. The signal S_{in} is subsequently split three times to equal parts. For visualization on an oscilloscope and each as input signal for the stand-alone bandpass filter and the R&F neuron. The output signal of the bandpass filter is evaluated by a spectrum analyzer as well as by the oscilloscope. The R&F neuron is evaluated in the time domain via the oscilloscope only. However, both devices are driven simultaneously, the spectrum of the bandpass filter can be used directly for monitoring the R&F neuron as well.

B. POST-SILICON VERIFICATION

We measured our fabricated chip to verify the circuit's functionality. First, as shown in Figure 7, we repeated the AC simulations measuring the stand-alone bandpass. Due to restrictions in the measurement setup, we limited our analysis to a studied frequency window of $f = 100 \text{ kHz} - 120 \text{ MHz}$. However, we consider this sufficient since the simulations show that the gain in higher frequency ranges is low as to be negligible. Frequencies below 100 kHz cannot be considered due to the measurement setup, but the gain response curve in that range should not be relevant either.

Figure 7a shows the measurement for tuning the resonant frequencies. We can recognize that tuning of the resonance frequencies is working. However, we observed two significant differences in the simulations. First, the measured maximum gain for each resonant frequency is lower than

the simulations. We attribute these losses partly to the measurement setup. On the other hand, to a second noticeable effect. All four resonance frequencies have a frequency shift of about $\Delta f = 145 - 190 \text{ kHz}$. As an explanation, we see here deviations due to tolerances in the manufacturing process. Manufacturing data of the present wafer confirm these assumptions. This is accompanied by the fact that the gain is designed for lower frequencies and thus there is also a loss in the maximum gain compared to the simulation. This results in new resonant frequencies at the following points: $G_{f0} = 1.05 \text{ MHz}$, $G_{f1} = 1.12 \text{ MHz}$, $G_{f2} = 1.19 \text{ MHz}$ and $G_{f3} = 1.26 \text{ MHz}$. Therefore, the frequency distance between each frequency is $\Delta f_{sep} = 70 \text{ kHz}$. However, the basic principles of the circuit work, and thus the demonstration of the encoding principle is still valid. In addition, the measurements for the tunable resonant frequencies are carried out with the maximum adjustable Q-factor. Until a frequency of approx. 35 MHz a clear curve profile is visible. After that frequency a difference to the previous profile of the curves can be seen. On the one hand, this can be attributed to the fact that the noise level converges in comparison to the reference peak. On the other hand, the sampling rate is lower in these areas.

In Figure 7b, we show the quality factor's adjustability principle. We focused on three different settings for clarity to validate the basic principle. We measured the setting for the maximum Q-factor, the lowest Q-factor, and a setting in between. Here, the maximum Q-factor is $G_{q0} = 11 \text{ dB}$, the lowest Q-factor is $G_{q2} = 0.2 \text{ dB}$, resulting in a difference of $\Delta G = 10.8 \text{ dB}$. Thus, the basic principle of the adjustability of the quality factor of the bandpass filter is also given. The characteristic of curves for higher frequencies corresponds

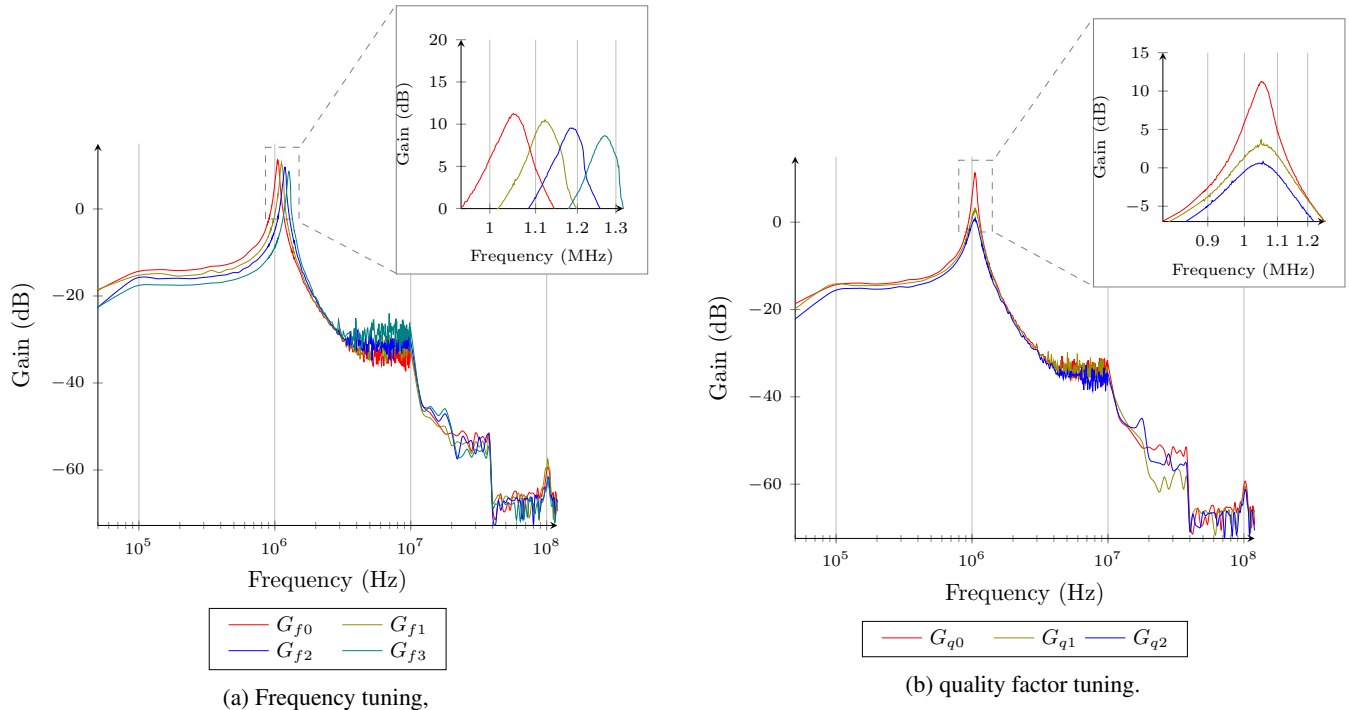


FIGURE 7: Measurements of the tuning options of the bandpass filter. In a), the adjustability of the frequencies over four different resonance points is shown, while in b), we show the adjustability of the quality factor in three of eight different options on the example of one resonance point.

to the considerations for the adjustability of the resonance frequency.

We can confirm the functionality of the bandpass filter by the measurements. However, a frequency difference occurs at the resonance frequencies compared to the simulations. Due to this and the measurement setup, the gain is lower than expected. In addition, we can show that despite this, the bandpass filter can be tuned for the resonance frequencies and the quality factor can be changed as expected.

To study the R&F neuron, we used a frequency generator to apply different sinusoidal waves with different frequencies corresponding to the resonance frequencies. As described before, the effect of the threshold gets relevant if there is no single wave applied but a combination of several signals. For this purpose, we first added two sinusoidal signals using a resistor network and applied them to the neuron. The functionality corresponds to the simulation, but for clarity, we omit the presentation of these measurements and concentrate on the encoding process. We are combining four different frequency generators and adding the signals using resistors. We consider the neuron individually. The network of four input neurons is recreated by considering the neuron with one setting over a certain period. At the same time, a spectrum analyzer is used to match the gain of the bandpass. By manually switching the resonance frequency, another neuron of the network is emulated. A neuron will generate a corresponding spike train depending on the applied input signal and the threshold. In Figure 8, we consider a signal summed up with

the following frequencies: $f_1 = 1.05$ MHz, $f_2 = 1.19$ MHz, $f_3 = 1.26$ MHz, and $f_4 = 1.33$ MHz. Thus, one resonant frequency is omitted in analogy to the simulation. For clarity, the evolution of the signal summed up is plotted over a larger time period than the neuron activity. In addition, we plot a signal with a scaling of a factor of 10 for illustration. The original signal appears noisy due to the low amplitude in the time domain and is therefore not easily recognizable. However, various test scenarios have shown that the low amplitude noise level is not a major challenge for the design and due to good filtering characteristics, these signals are correctly processed by the R&F neuron. The actual injected signal is correspondingly smaller in amplitude. Additionally, we consider the grayed-out area in the input signal for the spike trajectory. As expected, the signal produces a spike activity at neurons N_1 , N_3 , and N_4 , while neuron N_2 is without activity. Thus, the input signal is divided among the different neurons according to its frequency components. The difference in shape between simulated and measured spikes results from parasitic capacitive effects in the measurement setup which we verified by simulations.

In addition, signal leakages, as described in the simulations, can also lead to the neuron not recording individual periods if the threshold value is too high. A too-low threshold value can lead to the consequence that the neuron considers frequencies, which can be assigned to another neuron. However, the measurement results shown that the four R&F neurons represent three of the four frequencies.

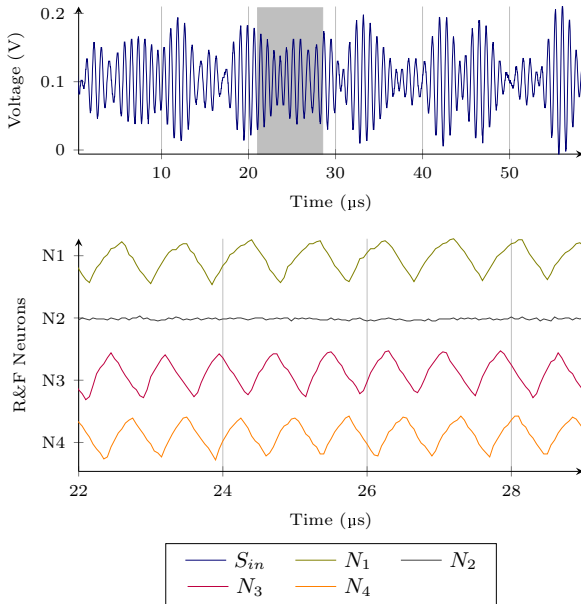


FIGURE 8: Measured encoding principle with four R&F neurons.

V. DISCUSSION, LIMITATIONS & CONCLUSION

In the next paragraphs, we will discuss our work. Following this, we will talk about limitations that emerge from our point of view and finally briefly conclude our work.

A. DISCUSSION

In this work we present one solution of the direct encoding of analog signals into spikes by converting the temporal domain into a spike-domain with the conversion into the frequency components. Therefore, the spike train represents the information in spatio-temporal events. The fundamental idea was first demonstrated by [16] with software simulations and the comparison with the FFT.

We first introduce the theoretical background of spiking neurons and the R&F model which acts like a frequency selective filter. Thus, we can categorize the encoding into the taxonomy of [18] as temporal coding in the subgroup filter-based. Important to understand that the rate of the spikes only appears due to the temporal existence of the signal and so the rate itself does not carry the information of the frequency but the spike itself. Additionally, we observed that the generated spike shape depends highly on the amplitude the neuron's threshold, realizing a variant of graded spikes similar to [33]. In a digital implementation such graded spikes would increase the communication between neurons heavily but in analog it is an inherent feature of the technology. However, there are solutions to generate invariant spike events with proper synaptic implementations.

[27] demonstrated the current injection encoding with Leaky Integrate-and-Fire (LIF) neurons which integrate the incoming current and generate a spike when the threshold is exceeded. The main difference between these two encoding

methods is in the inherent properties of the neuron. The R&F is superior because of its frequency selectivity, enabling the usage in various applications like speech recognition [43] or radar interference detection [17].

We verified the circuit implementation with simulations and hardware measurements of the fabricated chip. We demonstrated the successful continuous real-time conversion of sinusoidal signal to spatio-temporal spikes. In addition, but not shown in this paper, we have tested the circuit under extreme temperature conditions. We tested the functionality at -40°C as well as at 125°C . For both the cold temperature and the warm temperature, the functionality of the circuit is obtained. However, the temperature changes cause a degradation of the output gain of the bandpass filter. Accordingly, for full functionality of the R&F neuron, the threshold at the comparator must be adjusted.

Since this is the first R&F encoder in analog hardware there are still some challenges to solve which we further describe in the next section.

B. LIMITATIONS

As already mentioned besides the successful verification of the encoder functionality with analog R&F neurons, there still some challenges and improvements exist. We observed a few cases where the input frequencies of the input signal were either too close to each other or summed up improperly. As a result, a wrong neuron is also partially or even completely excited unless the threshold is accurately chosen. An adaptive threshold could be an approach for this problem. In addition, with the solution presented here, we can evaluate a relatively small frequency spectrum. For encoding multiple frequencies, we recommend implementing neurons with fixed resonance frequencies with optimized quality factors. Due to non-linear behavior of different components, a broad yield of resonance frequencies is challenging. An optimization to single frequency points would be the simplest solution. In addition, the measurements indicate that fabrication tolerances are also an important challenge. For a specific circuit that needs to select a certain spectrum of frequencies, an improvement in the robustness of manufacturing tolerances is indispensable. Additionally, challenging is the actual area consumption of a single neuron. To consider frequencies in the lower megahertz range, we need either large resistors or large capacitors. Both, however, consume a corresponding amount of area. An alternative way of implementing appropriate resonance frequencies would be preferable for integrating such circuits as encoding stages for SNNs. A possible solution for this could be the use of so-called pseudo-resistors [44]. These can be implemented relatively space-saving and with large resistance values. However, we suspect that this could lead to new problems regarding the stability of the system.

C. CONCLUSION

SNNs are expected to be a potentially exciting approach to achieve an energy-efficient and effective solution for data processing. To enable efficient signal processing with SNNs,

analog signals must be encoded from a temporal domain into a spiking domain. Various concepts are available for this purpose. One possibility is the R&F neurons, where a population acts like a frequency-selective filter bank. The individual neurons generate an output spike when the input signal components match the neuron's resonance frequency. This work demonstrated this current injection encoding with a novel circuit for the R&F neuron. We designed the circuit based on two fundamental circuits, a bandpass filter, and a comparator. First, we demonstrated the results of the R&F encoding scheme from a simulative basis and afterwards on an experimental basis with the fabricated circuit in a 130 nm BiCMOS technology. We show an approach for a direct analog to spike conversion with this neuron model, which can also be used as a hidden neuron in deeper network architectures. Nevertheless, we keep in mind some limitations and challenges that must be addressed to optimize the stability and performance of the R&F encoding.

•••

REFERENCES

- [1] A. Kugele, T. Pfeil, M. Pfeiffer, and E. Chicca, "Efficient processing of spatio-temporal data streams with spiking neural networks," *Frontiers in Neuroscience*, vol. 14, p. 439, 2020.
- [2] W. Maass, "Networks of spiking neurons: the third generation of neural network models," *Neural networks*, vol. 10, no. 9, pp. 1659–1671, 1997.
- [3] G. Debatt, T. Chauhan, B. R. Cotterreau, T. Masquelier, M. Paindavoine, and R. Baures, "Event-based trajectory prediction using spiking neural networks," *Frontiers in computational neuroscience*, p. 47, 2021.
- [4] N. K. Kasabov, *Time-space, spiking neural networks and brain-inspired artificial intelligence*. Springer, 2019.
- [5] M. Pfeiffer and T. Pfeil, "Deep Learning With Spiking Neurons: Opportunities and Challenges," vol. 12, p. 774. [Online]. Available: <https://www.ncbi.nlm.nih.gov/pmc/articles/PMC6209684/>
- [6] S. B. Furber, F. Galluppi, S. Temple, and L. A. Plana, "The spinnaker project," *Proceedings of the IEEE*, vol. 102, no. 5, pp. 652–665, 2014.
- [7] C. Mayr, S. Hoeppner, and S. Furber, "Spinnaker 2: A 10 million core processor system for brain simulation and machine learning," *arXiv preprint arXiv:1911.02385*, 2019.
- [8] M. Davies, N. Srinivasa, T.-H. Lin, G. Chinya, Y. Cao, S. H. Choday, G. Dimou, P. Joshi, N. Imam, S. Jain *et al.*, "Loihi: A neuromorphic manycore processor with on-chip learning," *Ieee Micro*, vol. 38, no. 1, pp. 82–99, 2018.
- [9] A. Neckar, S. Fok, B. V. Benjamin, T. C. Stewart, N. N. Oza, A. R. Voelker, C. Eliasmith, R. Manohar, and K. Boahen, "Braindrop: A mixed-signal neuromorphic architecture with a dynamical systems-based programming model," *Proceedings of the IEEE*, vol. 107, no. 1, pp. 144–164, 2018.
- [10] C. Frenkel, M. Lefebvre, J.-D. Legat, and D. Bol, "A 0.086-mm² 12.7-pj/sop 64k-synapse 256-neuron online-learning digital spiking neuromorphic processor in 28-nm cmos," *IEEE Transactions on Biomedical Circuits and Systems*, vol. 13, no. 1, pp. 145–158, 2019.
- [11] J. Stuijt, M. Sifalakis, A. Yousefzadeh, and F. Corradi, "μbrain: An event-driven and fully synthesizable architecture for spiking neural networks," *Frontiers in neuroscience*, p. 538, 2021.
- [12] P. S. Diniz, E. A. Da Silva, and S. L. Netto, *Digital signal processing: system analysis and design*. Cambridge University Press, 2010.
- [13] J. Schemmel, S. Billaudelle, P. Dauer, and J. Weis, "Accelerated Analog Neuromorphic Computing," *arXiv*, Tech. Rep., arXiv:2003.11996 [cond-mat, q-bio] type: article. [Online]. Available: <http://arxiv.org/abs/2003.11996>
- [14] S. Furber, "Large-scale neuromorphic computing systems," *Journal of neural engineering*, vol. 13, no. 5, p. 051001, 2016.
- [15] E. M. Izhikevich, "Resonate-and-fire neurons," *Neural networks*, vol. 14, no. 6-7, pp. 883–894, 2001.
- [16] D. Auge and E. Mueller, "Resonate-and-fire neurons as frequency selective input encoders for spiking neural networks," 2020.
- [17] J. Hille, D. Auge, C. Grassmann, and A. Knoll, "Resonate-and-fire neurons for radar interference detection," in *Proceedings of the International Conference on Neuromorphic Systems 2022*, 2022, pp. 1–4.
- [18] D. Auge, J. Hille, E. Mueller, and A. Knoll, "A Survey of Encoding Techniques for Signal Processing in Spiking Neural Networks," *Neural Processing Letters*, Jul. 2021.
- [19] E. D. Adrian and Y. Zotterman, "The impulses produced by sensory nerve endings," vol. 61, no. 4, pp. 465–483.
- [20] C. M. Gray, P. König, A. K. Engel, and W. Singer, "Oscillatory responses in cat visual cortex exhibit inter-columnar synchronization which reflects global stimulus properties," vol. 338, no. 6213, pp. 334–337. [Online]. Available: <https://www.nature.com/articles/338334a0>
- [21] F. Theunissen and J. P. Miller, "Temporal encoding in nervous systems: a rigorous definition," *Journal of computational neuroscience*, vol. 2, pp. 149–162, 1995.
- [22] K. H. Srivastava, C. M. Holmes, M. Vellema, A. R. Pack, C. P. Elemans, I. Nemenman, and S. J. Sober, "Motor control by precisely timed spike patterns," *Proceedings of the National Academy of Sciences*, vol. 114, no. 5, pp. 1171–1176, 2017.
- [23] W. Gerstner, W. M. Kistler, R. Naud, and L. Paninski, *Neuronal dynamics: From single neurons to networks and models of cognition*. Cambridge University Press, 2014.
- [24] B. Rueckauer and S.-C. Liu, "Conversion of analog to spiking neural networks using sparse temporal coding," in *2018 IEEE international symposium on circuits and systems (ISCAS)*. IEEE, 2018, pp. 1–5.
- [25] J. J. Hopfield, "Pattern recognition computation using action potential timing for stimulus representation," vol. 376, no. 6535, pp. 33–36. [Online]. Available: <https://www.nature.com/articles/376033a0>
- [26] P. Lichtsteiner, C. Posch, and T. Delbrück, "A 128x128 120 dB 15 μs Latency Asynchronous Temporal Contrast Vision Sensor," vol. 43, no. 2, pp. 566–576.
- [27] H. M. Lehmann, J. Hille, C. Grassmann, A. Knoll, and V. Issakov, "Analog spiking neural network based phase detector," *IEEE Transactions on Circuits and Systems I: Regular Papers*, vol. 69, no. 12, pp. 4837–4846, 2022.
- [28] L. Osborn, H. Nguyen, R. Kaliki, and N. Thakor, "Prosthesis grip force modulation using neuromorphic tactile sensing," in *Myoelectric Controls Symposium (University of New Brunswick, 2017)*, 2017, pp. 188–191.
- [29] S.-C. Liu and T. Delbrück, "Neuromorphic sensory systems," *Current opinion in neurobiology*, vol. 20, no. 3, pp. 288–295, 2010.
- [30] T. Birkben, H. Winterfeld, S. Fichtner, A. Petrucci, and H. Kohlstedt, "A spiking and adapting tactile sensor for neuromorphic applications," *Scientific reports*, vol. 10, no. 1, p. 17260, 2020.
- [31] K. Nakada, T. Asai, and H. Hayashi, "A silicon resonate-and-fire neuron based on the volterra system," in *Int. symp. on nonlinear theory and its applications*, 2005, pp. 82–85.
- [32] M. A. Azam, D. Bhattacharya, D. Querlioz, and J. Atulasimha, "Resonate and fire neuron with fixed magnetic skyrmions," *Journal of Applied Physics*, vol. 124, no. 15, p. 152122, 2018.
- [33] G. Orchard, E. P. Frady, D. B. D. Rubin, S. Sanborn, S. B. Shrestha, F. T. Sommer, and M. Davies, "Efficient neuromorphic signal processing with loihi 2," in *2021 IEEE Workshop on Signal Processing Systems (SiPS)*. IEEE, 2021, pp. 254–259.
- [34] M. Shayegannia and H. Al-Nashash, "Low frequency filter design using gyrator for biomedical applications," in *Proceedings of the 4th IEEE GCC Conference*, 2007, pp. 1–4.
- [35] R. Schaumann, X. Mac Elwyn Van Valkenburg, and H. Xiao, *Design of analog filters*. Oxford University Press New York, 2001, vol. 1.
- [36] C. Schenk and U. Tietze, *Halbleiterschaltungstechnik*. Springer, 1993.
- [37] K. L. Su, *Analog filters*. Springer Science & Business Media, 2012.
- [38] A. B. Williams, *Analog filter and circuit design handbook*. McGraw-Hill Education, 2014.
- [39] H. M. Lehmann, J. Hille, C. Grassmann, and V. Issakov, "Spiking neural networks based rate-coded logic gates for automotive applications in bicosmos," in *2021 IEEE International Conference on Microwaves, Antennas, Communications and Electronic Systems (COMCAS)*. IEEE, 2021, pp. 280–285.
- [40] M. Rozenberg, O. Schneegans, and P. Stolar, "An ultra-compact leaky-integrate-and-fire model for building spiking neural networks," *Scientific reports*, vol. 9, no. 1, p. 11123, 2019.
- [41] H. M. Lehmann, J. Hille, C. Grassmann, and V. Issakov, "Leaky integrate-and-fire neuron with a refractory period mechanism for invariant spikes," in *2022 17th conference on Ph. D research in microelectronics and electronics (PRIME)*. IEEE, 2022, pp. 365–368.

- [42] V. Kornijcuk, H. Lim, J. Y. Seok, G. Kim, S. K. Kim, I. Kim, B. J. Choi, and D. S. Jeong, "Leaky integrate-and-fire neuron circuit based on floating-gate integrator," *Frontiers in neuroscience*, vol. 10, p. 212, 2016.
- [43] D. Auge, J. Hille, F. Kreutz, E. Mueller, and A. Knoll, "End-to-end spiking neural network for speech recognition using resonating input neurons," in *Artificial Neural Networks and Machine Learning – ICANN 2021*, I. Farkaš, P. Masulli, S. Otte, and S. Wermter, Eds. Cham: Springer International Publishing, 2021, vol. 12895, pp. 245–256.
- [44] E. Guglielmi, F. Toso, F. Zanetto, G. Sciotino, A. Mesri, M. Sampietro, and G. Ferrari, "High-value tunable pseudo-resistors design," *IEEE Journal of Solid-State Circuits*, vol. 55, no. 8, pp. 2094–2105, 2020.



HENDRIK M. LEHMANN received the B.Sc. and M.Sc. in Electrical Engineering and Business Administration in 2018 and 2019 from the CAU Kiel, Germany. He joined Infineon Technologies AG in Neubiberg, Germany in 2020 as a researcher and is currently pursuing his Ph.D. in collaboration with the Technical University of Braunschweig, Germany. His research interests are in the area of analog circuit design with a focus on Spiking Neural Networks and their integration abilities in sensor-related applications.



JULIAN HILLE earned his B.Eng. in Electrical Engineering in 2017 at the University of Applied Sciences in Augsburg, Germany, and since 2019 he holds an M.Sc. in Electronic Design from Lund University, Sweden. Currently, he is a researcher at Infineon Technologies AG in Neubiberg, Germany, and pursuing his Ph.D. in collaboration with the Technical University of Munich, Germany. The primary focus of his research is about near-sensor processing with Spiking Neural Networks and the conversion of temporal data to spike representation.



CYPRIAN GRASSMANN received his Diploma in Electrical and Electronics Engineering in 1995 from RWTH Aachen University, Germany and his Ph.D. in 2003 from the Friedrich-Wilhelms-University Bonn, Germany. He was with Infineon Technologies AG, Munich & Neubiberg, Germany from 2001 to 2011. Afterwards he worked for Intel Mobile Communications GmbH, Neubiberg, Germany until 2016 before rejoining Infineon Technologies AG. He is currently a distinguished engineer at Infineon for Automotive Radar Systems, and he also explores the potential of neuromorphic solutions for automotive radar applications.



VADIM ISSAKOV (Senior Member, IEEE) received the M.Sc. degree in microwave engineering from the Technical University of Munich, Munich, Germany, in 2006, and the Ph.D. degree (*summa cum laude*) from the University of Paderborn, Germany, in 2010. In March 2010, he joined Infineon Technologies AG, Neubiberg, Germany. Afterwards, he worked at imec, Leuven, Belgium, and Intel Corporation, before he came back to Infineon Technologies AG in August 2015 as a millimeter-wave (mm-Wave) design lead and principal engineer leading a research group working on predevelopment of mm-Wave radar and communication products. Since 2014, he has been a guest lecturer with Ruhr-University Bochum, Germany, and the University of Erlangen, Germany. In September 2019, he joined the University of Magdeburg, Germany as a full professor holding the chair for Electronics. Since April 2021, he has been working as a full professor with Technical University Braunschweig, Germany. His research interests include mm-Wave circuits, RF systems, mm-Wave measurement techniques, and RF-ESD. He has authored or co-authored over 125 peer-reviewed papers, one book, and holds 11 patents. Dr. Issakov was a recipient of the 2010 University of Paderborn best Dissertation Award, 2011 VDI/VDE distinguished dissertation award, and a 2019 IEEE MTT Outstanding Young Engineer Award. He serves as Associate Editor of the T-MTT and MWCL and also on the technical program committees of RFIC and BCICTS. He is also the distinguished lecturer of the IEEE Microwave Theory and Technique Society in 2023-2025.